*Journal of Ceramic Processing Research. Vol. 20, Special. 1, pp. s92~s99 (2019)*
*(Received 9 December 2018, Received in revised form 11 January 2019, Accepted 11 January 2019)*

J O U R N A L O F
**Ceramic Processing Research**

# Enhancement of thermal and insulation properties of $\alpha$-$Al_2O_3$/PAI hybrid materials prepared by surface-modified $\alpha$-$Al_2O_3$

**Ho Seong Na[a,b], Hyung Mi Lim[a], Dae Su Jung[a], Seung-Ho Lee[a], Dong Kyu Roh[a], Deug Joong Kim[b] and Dae-Sung Kim[a,*]**
[a]*Energy Environment Division, Korea Institute of Ceramic Engineering & Technology (KICET) Jinju-si, Gyeongsangnam-do 52851, Korea*
[b]*School of Advanced Materials Science & Engineering, Sungkyunkwan University, Suwon 16419, Korea*

**To improve α-$Al_2O_3$ dispersion and increase the possible interaction between α-$Al_2O_3$ and a polyamideimide (PAI) matrix, the α-$Al_2O_3$ surface was modified with different amounts of a silane coupling agent, N-phenyl-(3-aminoproyl)trimethoxy silane (N-APTMS). Surface-modified α-$Al_2O_3$ was successfully functionalized with N-APTMS through a binary solvent system. To confirm and modify the amount of silane precisely, the OH site density on α-$Al_2O$ was measured through acid-base titration as 1.001, 2.537, and 0.980 OH/nm$^2$ for pristine (A-O), ball-milled (A-M), and surface-modified (A-SM-100) α-$Al_2O_3$, respectively. The surface-modified α-$Al_2O_3$ was dispersed in N-methyl-2-pyrrolidone (NMP) and the solutions were fully mixed in PAI resin. The A-SM/PAI were coated on Cu plate and thermally cured. The thermal conductivity and dielectric breakdown strength of A-SM/PAI film on Cu plate were greater than those of pristine PAI or pristine hybrid material.**

**Key words: Organic-inorganic hybrid material, α-$Al_2O_3$, OH site density, Silane coupling agent, Thermal properties.**

## Introduction

The development of organic-inorganic hybrid materials for achieving improved physicochemical properties is rooted in the interactions between organic polymers and inorganic materials. Organic-inorganic hybrid materials combine the advantages of low weight, process diversity, heat resistance, and electrical insulation of organic polymers and the advantages of corrosion resistance, wear resistance, thermal conductivity, and thermal stability of inorganic oxides, and they have been studied extensively in a variety of fields including electronic materials, biocompatible materials, paint and optical films, and electrical insulating materials [1-4]. The most important factor for improving the properties of an organic-inorganic hybrid material is the formation, size, and dispersibility of the inorganic oxide particles. In particular, it has been reported that, when nanosized inorganic particles are uniformly dispersed in the dispersion medium and the surface area increases, their properties are greatly improved compared to those of micro-particles [1, 5, 6]. Nanoparticles may show varying properties depending on their type and size, and when nanoparticles are hybridized within an organic polymer, they can improve the functions of the organic polymer itself. However, as the sizes of inorganic particles approach the nanoscale, the surface energy of the particles increases and they lose their affinity to organic polymers, causing agglomeration or aggregation among inorganic particles [4, 6-8]. Accordingly, the decrease of the repulsive force between particles through chemical surface treatment is known to be important for the dispersion of nanoparticles within solvents or organic polymers.

The dispersion of typical nanoparticles is achieved through a mechanical milling process that has high energy, the nanoparticles high energy, and a stable dispersion sol can be prepared by chemically controlling the hydrogen ion concentration and strength to reduce the repulsive force between particles caused by electro-static, steric hindrance, and/or electro-static hindrance [9]. One of the well-known methods for increasing their affinity for organic polymers is the use of a surfactant, dispersant, organic acid, or silane coupling agent that can bind to the reacting group of the organic polymer [9, 10].

P. Jiang et al. discussed the enhancement of properties achieved by applying surface-modified $Al_2O_3$ on epoxy resin at high temperature using xylene as a single solvent together with a silane coupling agent [11]. However, because the dispersibility of non-polar xylene and polar inorganic material is significantly reduced during surface modification, the amount of silane coupling agents adsorbed locally on the particle surface is relatively low. Therefore, the particle behavior in solvent has a very important influence during surface modification. Hydroxyl groups that can form bonds through chemical surface treatment are

*Corresponding author:
Tel : +82-55-792-2453
Fax: +82-55-792-2579
E-mail: dskim@kicet.re.kr

present on the inorganic oxide surface, and the number of hydroxyl groups varies depending on the type and preparation method of the inorganic oxide. For improving the properties of organic-inorganic hybrid materials, we have continuously studied methods to control the particle-particle repulsive force of inorganic particles in organic-inorganic hybrid materials via the preparation of inorganic particles of different sizes and shapes, preparation of dispersion sol through milling, pH control, and the use of additives such as dispersants and stabilizing ions [12-14]. Furthermore, we recently reported colloidal silica produced by 3 different methods showing different numbers of hydroxyl groups [15]. Therefore, because the number of hydroxyl groups that can react determines the amount of silane coupling agent that bonds and is also directly linked to improvement in the physical properties of the final product, it is important to understand the surface properties of inorganic oxides [15].

In the present study, α-$Al_2O_3$ with excellent thermal conductivity and insulation properties was used as the starting material for preparing α-$Al_2O_3$/PAI organic-inorganic hybrid material with enhanced thermal properties achieved through silane surface modification. The surface modification process was optimized by analyzing the correlation between the number of OH sites on the α-$Al_2O_3$ particle surface and the adsorbed amount of surface-modified silane. In particular, the dispersion properties of α-$Al_2O_3$ with surface modification using N-Phenyl-(3-aminopropyl)trimethoxy silane (N-APTMS) under a binary solvent were observed within N-methyl-2-pyrrolidone (NMP) solvent. Moreover, the thermal conductivity and insulation properties of the polyamideimide (PAI) hybrid material consisting of PAI resin and α-$Al_2O_3$ were observed before and after surface modification. The correlation between thermal and insulation properties is discussed in terms of dispersion and whether inorganic material was added into PAI resin.

## Experimental Method

### Materials

The commercial α-$Al_2O_3$ nano sol (AKP-53) was purchased from Sumitomo, Japan. Anhydrous ethanol (99.5%), 1,3-dimethylbenzene (xylene, 98.5%) N-methyl-2-pyrrolidone (NMP, 99.5%) and nitric acid ($HNO_3$, 60%) were purchased from Daejung Chemical Co., Korea. N-phenyl-(3-aminopropyl)trimethoxy silane (N-APTMS) was purchased from Aldrich. All chemicals were used as received without further purification.

### Preparation of α-$Al_2O_3$ nano sol (A-M)

The α-$Al_2O_3$ nano sol was prepared by milling process. The α-$Al_2O_3$ nanoparticles were dispersed by batch-type sand mill (Alesco, Japan) equipped with an alumina disk having a diameter of 70 mm. Anhydrous ethanol and nitric acid were used as the solvent and dispersant, respectively. Milling process was performed for 3 hrs by using zirconia beads, which were a 1:1 mixture of beads having sizes of 0.1 and 0.3 mm. The concentration of the prepared α-$Al_2O_3$ nano sol was approximately 5 wt%.

### Surface modification of α-$Al_2O_3$ (A-SM)

For the surface modification of α-$Al_2O_3$ with hydrophobic N-APTMS, the prepared α-$Al_2O_3$ nano sol with a solid content of 5wt% was transferred into a three-necked flask fitted with a reflux condenser, following which xylene was added in the dispersion solution. Subsequently, the amount of N-APTMS to be added was calculated based on the specific surface area of α-$Al_2O_3$ and minimum covering area of N-APTMS, as expressed in the equation below [16].

$$\text{APTMS(wt\%)} = \frac{Weight\ of\ Al_2O_3(wt\%) \times Specific\ Sur\ face\ Area\ of\ Al_2O_3(m^2/g)}{Minimum\ covering\ area\ of\ APTMS(m^2/g)} \quad (1)$$

The mixture was heated to 120 °C to remove the ethanol of solution, and then allowed to react by stirring for 6 hrs. After the reaction had completed, the surface-modified α-$Al_2O_3$ (A-SM) nanoparticles were washed several times with xylene and ethanol, and the dried in a vacuum oven at 120 °C for 12 hrs.

### Preparation of A-SM/PAI hybrid coating film

To prepare the A-SM/PAI hybrid coating solution, the surface-modified α-$Al_2O_3$ nano particles were dispersed in NMP, and then PAI dissolved in dispersion solution. The concentration of final hybrid coating solution was 20wt%. This solution was evenly coated on a Cu substrate using a spin coater followed by thermally cured at 200 °C for 40 min to produce the coating film.

### Characterization

Crystalline phase analysis of the α-$Al_2O_3$ powder was performed using an X-ray diffractometer (XRD, Dmax2500, Rigaku) with an acceleration voltage of 40 kV, current of 200 mA, scan speed of 5 °/min, and in the range of $2\theta = 5 \sim 90$ °. The shapes and sizes of the particles were observed using a 200kV transmission electron microscope (TEM, JEM-2000EX, JEOL, Japan), while a dynamic light-scattering spectrophotometer (ELS-Z, Otsuka Electronics, Japan) was used to measure the average particle size and particle distribution. The specific surface area of the particles was measured after pretreating approximately 0.2 g of the powder for 12 hrs at 180 °C under vacuum condition using the Brunauer-Emmett-Teller (BET, Tristar 3000, Micromeritics) method based on nitrogen adsorption/desorption. The silane content adsorbed on the particle surface was analyzed before and after surface modification via thermogravimetric

analysis (TGA, Mettler Toledo STARe System). The measurements were taken in air at a heating rate of 5 °C/min, and the values were converted to percentages at a range of 25-1000 °C for observing content changes. For observing the hydrophilicity and hydrophobicity of the powder before and after the surface modification, a wettability analyzer (Sigma700/701) was used to identify the weight change generated from placing 1 g of α-$Al_2O_3$ powder in a cylindrical container and then immersing the container in water.

The density of hydroxyl groups on the surface of α-$Al_2O_3$ particles was measured before and after surface modification by using an acid/base titrator (719-S Titrino, Metrohm), and the number of hydroxyl groups on the surface was calculated based on the study results by J.W. Ntalikwa, [17] and H. Tang [18]. To compare the samples against each other, the specific surface area was set to 80 $m^2$/g, and the calculated particles were prepared by diluting with 0.1 M NaCl. Moreover, the samples were stirred for 12 hrs at a speed of 50 cc/min, under $N_2$ gas (99.95%) atmosphere, to eliminate any $CO_2$ in the solution before performing the analysis. Next, it was titrated to pH 5 with 0.1 M HCl and then back-titrated up to pH 10 with 0.05 M NaOH at a rate of 0.02 ml/min. The calculated graph was converted to a gran plot for the calculation of surface charge density ($H_s$) and surface site density ($D_s$).

The A-SM/PAI hybrid composite was coated on the Cu substrate (6 × 6 cm) by using spin coating at 2500 rpm. First, primer was coated and then α-$Al_2O_3$/PAI hybrid composite was coated twice or three times to control coating thickness. The coated films on the Cu substrate were cured at 200 °C for 40 min. The samples were bended for bending test using spacer of 0.5 mm and then pressed at 1 ton. Then the bent part of coated sheet was observed with an optical microscope (POM, ECLIPSE LV100) [13].

A withstanding voltage tester (TOS 5101, KIKUSUI) was used to measure the organic-inorganic hybrid coating film according to its thickness. A pulsed-laser-type thermal conductivity meter (LFA 427, Netzch) was used to measure the thermal conductivity, while the sample ring was fabricated by transferring the coating sol to a silicone mold and hardening at 160 °C.

## Results and Discussion

### Properties of α-$Al_2O_3$ nano sol

To prepare well dispersed α-$Al_2O_3$ nano sol, the commercial α-$Al_2O_3$ was broken to small size nanoparticles by bead milling. Transmission electron microscopy (TEM) images of α-$Al_2O_3$ nanoparticles before and after bead milling are shown in Fig. 1. The pristine α-$Al_2O_3$ particles before bead milling, it showed a distribution of coarse particles with a size of approximately 300 nm in Fig. 1(a). After bead milling for 3hrs, the size of alumina nanoparticles decreased down to

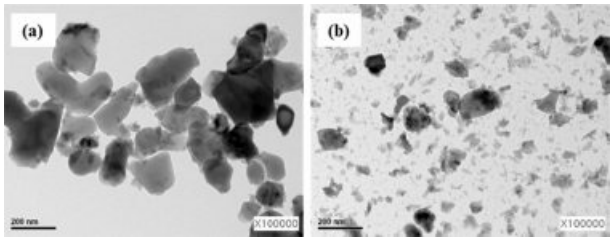


**Fig. 1.** TEM images of α-$Al_2O_3$ (a) before and (b) after bead milling.

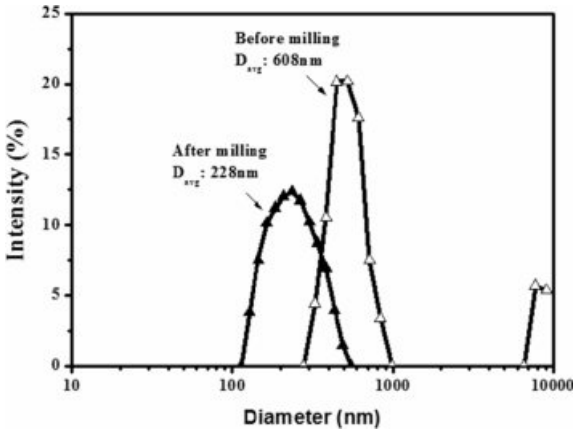


**Fig. 2.** Particle size distribution of α-$Al_2O_3$ (a) before and (b) after bead milling.

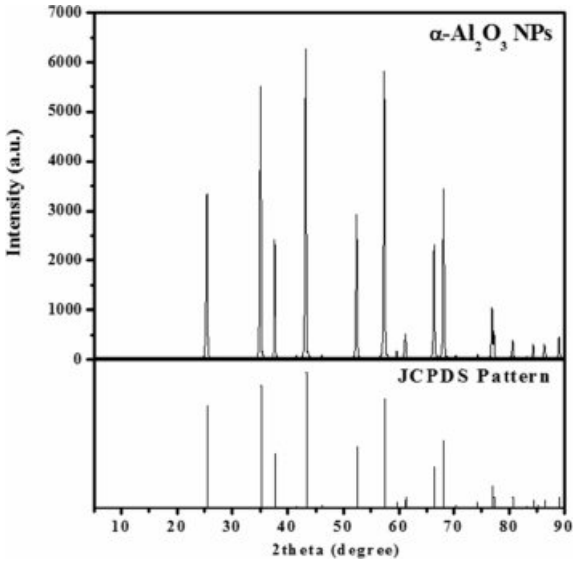


**Fig. 3.** XRD pattern of α-$Al_2O_3$ powder.

30 nm. Fig. 1(b) showed a composition consisting of a mixture of coarse α-$Al_2O_3$ particles in the range of 30 nm to 200 nm particles. Although nonpulverized particles with a few hundred nm still exist, most of particles show tens-of-nanometer size. It is believed that the decrease of the size of α-$Al_2O_3$ particles to the nano-scale through bead milling could increase the specific surface area

and the number of hydroxyl groups on the particle surface, resulting in changes in the site and amount of silane surface modification.

Fig. 2 shows the results of particle-size analysis performed on pre-milling and post-milling of α-$Al_2O_3$ nanoparticles. The average particle size decreased from 608 nm to 228 nm after milling, allowing dispersion sol with relatively narrow particle size distribution to be prepared. In the present study, coarse particles were used as-is without removing them, but when coarse particles were moved, the average particle size decreased to approximately 150 nm. The bead-milled alumina nanoparticles were dispersed in ethanol and used for silane surface modification.

The crystal structure of alumina nanoparticles was characterized by using XRD analysis in the 2θ range of 5 ° to 90 °, as shown in Fig. 3. The diffraction peaks in the XRD patterns indicated that $Al_2O_3$ and M-$Al_2O_3$ are α phase of alumina. Peaks at 25.8, 35.1, 37.5, 43.1, 52.3, 57.3, 66.3, and 67.9 ° correspond to the reflections from the (012), (104), (110), (113), (024), (116), (214), and (300) crystal planes of α-$Al_2O_3$, respectively (JCPDS No. 10-0173).

## Study of α-$Al_2O_3$ surface properties before and after silane surface modification

Fig. 4 shows the TGA, wettability, and PSA results of surface-modified α-$Al_2O_3$ according to the N-APTMS content as calculated using Equation (1). In Fig. 4(a), the pure α-$Al_2O_3$(A-O) showed a low heat loss of 0.73%, but when surface modification was performed according to the N-APTMS content, the heat loss of surface-modified α-$Al_2O_3$ (A-SM) increased. A-SM-50(50%), A-SM-100(100%), and A-SM-200(200%) showed heat losses of 3.3, 3.6, and 1.4%, respectively. In Fig. 4(b), hydrophilicity is seen as the absorption of a greater amount of water, and hydrophobicity is seen as the absorption of a lower amount of water is absorbed. The water absorption amount of A-O was 0.65 g, while the water absorption amount of A-SM-50, A-SM-100, and A-SM-200 were 0.11, 0.04, and 0.38 g, respectively because of N-APTMS modification. Fig. 4(c) shows the results of particle distribution of surface-modified α-$Al_2O_3$ in NMP. The mean particle size of A-O was 580 nm, while those of A-SM-50, A-SM-100, and A-SM-200 were 93, 89, and 134 nm, respectively, indicating that the A-SM-100 samples showed very stable dispersibility in NMP solvent. Without surface modification, α-$Al_2O_3$ nanoparticles were easily aggregated in NMP.

The A-SM-50 and A-SM-100 samples showed increased adsorption on the particle surface with increasing silane content, whereas the A-SM-200 sample showed decreased adsorption rate with increasing silane content. It is believed that this is due to the speed of silanes reacting amongst themselves being higher than the speed of the reaction on the particle surface according to the amount of silane being added, resulting in a reduced amount of silane absorbed on the surface.

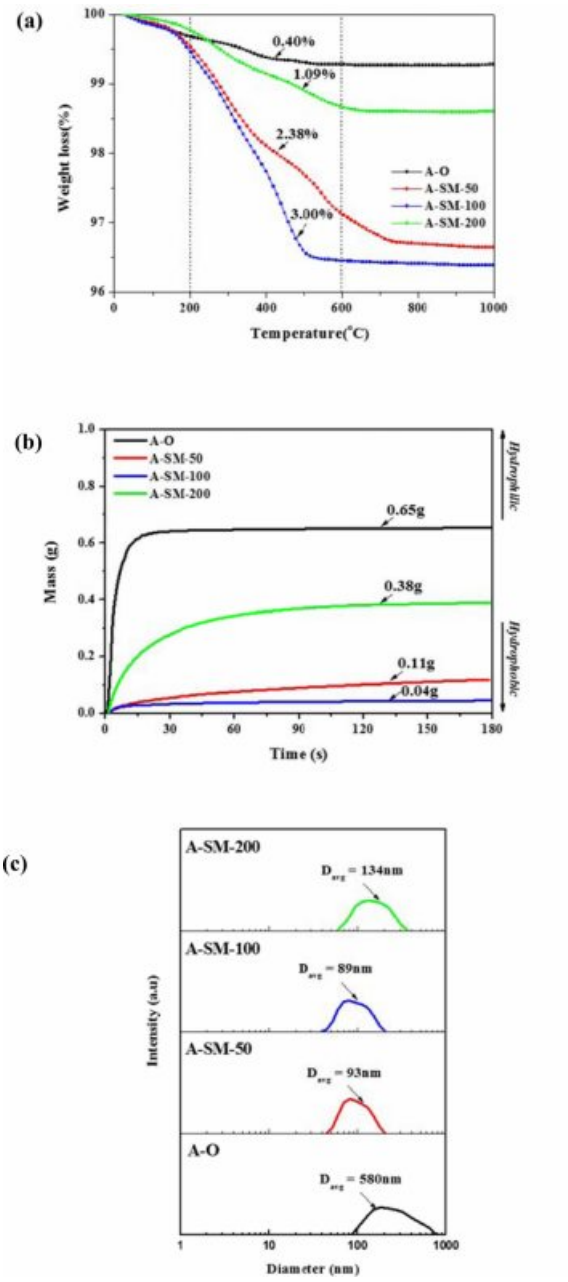


**Fig. 4.** Characterization of surface-modified α-$Al_2O_3$ according to the silane content: (a) TGA curves, (b) water wettability, and (c) particle size distribution.

For examining the correlations of surface modification according to the surface characteristics of α-$Al_2O_3$, each sample for A-O, A-M, and A-SM was subjected to acid-base titration. Accordingly, process of back titration can be divided into 3 sites: the acidic site with excess acid, the site where reaction with the particle surface occurs, and the alkaline site with excess base. The volumes of these sites can be calculated by taking the back-titration data from the titration experiment and drafting a gran plot using the gran function (*G*), with the gran function values shown below [15].

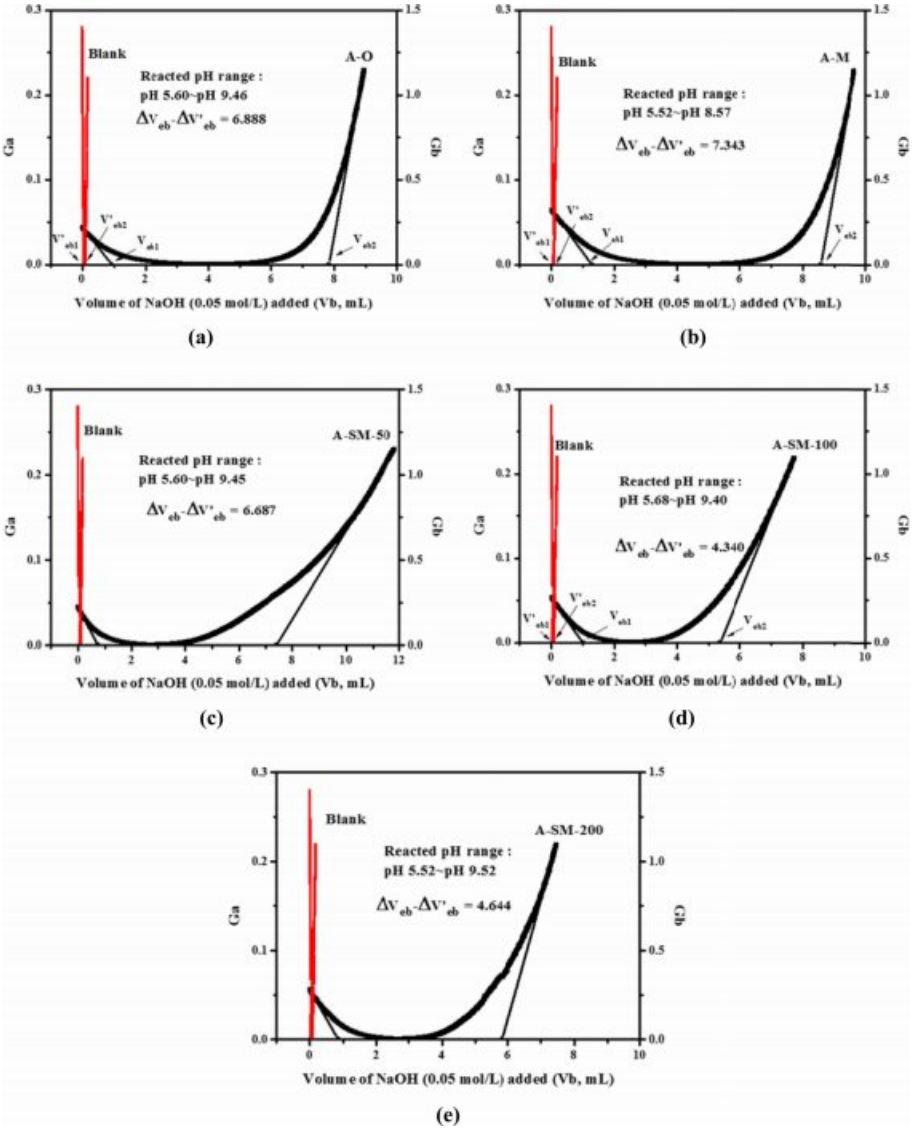


**Fig. 5.** Gran plot of α-$Al_2O_3$ calculated by acid-base titration: (a) A-O, (b) A-M, (c) A-SM-50, (d) A-SM-100, and (e) A-SM-200.

On the acidic site: $Ga = (V_0 + V_{at} + V_b) \cdot 10^{-pH} \cdot 100$ (2)

On the alkaline site: $Gb = (V_0 + V_{at} + V_b) \cdot 10^{-(13.8-pH)} \cdot 100$ (3)

Here, $V_0$ represents the initial volume of the dispersion sol sample, $V_{at}$ represents the total volume of acid added, and $V_b$ represents the volume of base added. By using a linear regression analysis of slopes from the gran plot of the blank solution and samples plotted using Equations (2) and (3), the volume of the site where all acid is consumed ($V_{eb1}$) and that of the site where base is added ($V_{eb2}$) can be derived, and the volume reacting on the particle surface can be calculated. From these values, the values of $H_s$ and $D_s$ were calculated.

$$Hs = \frac{(V_{eb2} - V_{eb1})sample \cdot C_b - (V_{eb2} - V_{eb1})blank \cdot C_b}{V_0} (\text{mol } L^{-1}) \quad (4)$$

**Table 1.** Surface site concentration (*Hs*) and surface site density (*Ds*) of α-$Al_2O_3$ calculated using the gran plot of Fig. 4.

| Sample name | Materials | Amount of silane (%) | SSA ($m^2$/g) | Hs (mmol/L) | Ds (-OH/ $nm^2$) |
|---|---|---|---|---|---|
| A-O | α-$Al_2O_3$ | - | 13.73 | 3.226 | 1.001 |
| A-M | α-$Al_2O_3$ Milling | - | 22.12 | 6.119 | 2.537 |
| A-SM-50 | Modified α-$Al_2O_3$ | 50 | 21.11 | 4.456 | 1.221 |
| A-SM-100 | Modified α-$Al_2O_3$ | 100 | 25.84 | 3.617 | 0.980 |
| A-SM-200 | Modified α-$Al_2O_3$ | 200 | 18.39 | 4.120 | 1.350 |

Here, $C_b$ is the concentration of NaOH.

$D_s$ can be calculated using the following equation:

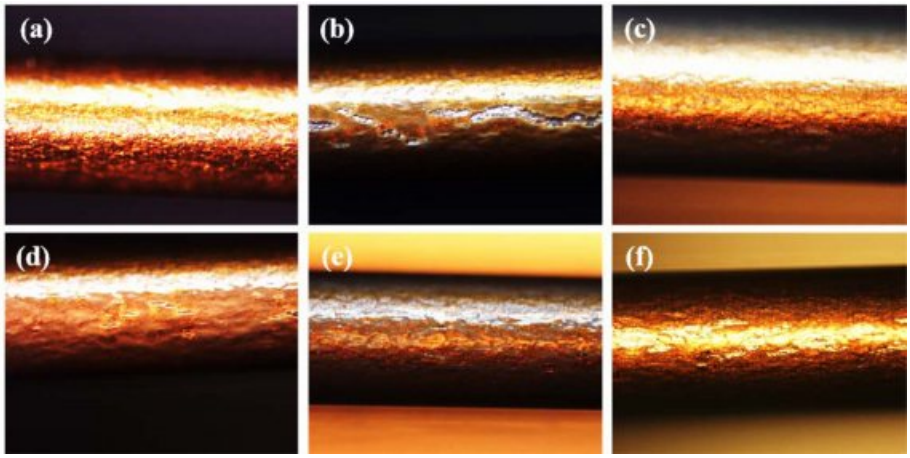


**Fig. 6.** Optical microscope images of the coating films for observing the fracture after bending test of α- $Al_2O_3$/PAI hybrid composites (20wt%) at 0.4 mm: (a) PAI only, (b) A-O, (c) A-M, (d) A-SM-50, (e) A-SM-100, and (f) A-SM-200.

$$Ds = \frac{(H_S \cdot N_A)}{S_{BET} \cdot C_P \cdot 10^{18}} (sites\ nm^{-1}) \quad (5)$$

Here, $N_A$ is Avogadro's number ($6.022 \cdot 10^{23}$ sites $mol^{-1}$), $S_{BET}$ represents the specific surface area of the particles, and $Cp$ represents the particle concentration.

The gran plot results of A-O, A-M, and A-SM samples were shown in Fig. 5(a-e). From the slopes of the measured samples and the blank, $V_{eb}$ and $V'_{eb}$ were derived via a linear regression analysis. $H_s$ and $D_s$ calculated from Equations (4) and (5) are listed in Table 1. The densities of surface hydroxyl groups of A-O and A-M samples were 1.001 and 2.537 OH/$nm^2$, respectively, indicating a significant increase in surface hydroxyl groups due to reduced particles size. Meanwhile, the densities of surface hydroxyl groups of α-$Al_2O_3$ with surface modification using A-SM-50, A-SM-100, and A-SM-20 decreased to 1.221, 0.980, and 1.350 OH/$nm^2$, respectively. It can be concluded that A-SM-100, with the fewest number of surface sites, underwent the greatest amount of surface modification. Correlations were found with the results of TGA, wettability, and PSA shown in Fig. 4, which also showed that the surface modification directly influences the behavior of $Al_2O_3$ within NMP according to the content of the silane coupling agent.

## Thermal conductivity and insulation properties of A-SM/PAI hybrid coating film

Fig. 6 shows an image of the fracture of the coating film by a bending test of α-$Al_2O_3$/PAI hybrid composite with 20 wt% loading films. It was observed that some cracks were generated in A-O/PAI coating films after bending test. However, the cracks reduced and disappeared in the well modified A-SM/PAI coating films due to high dispersibility of nanofiller in PAI matrix and low surface resistance between nanofiller and PAI matrix result in improvement of bending durability.

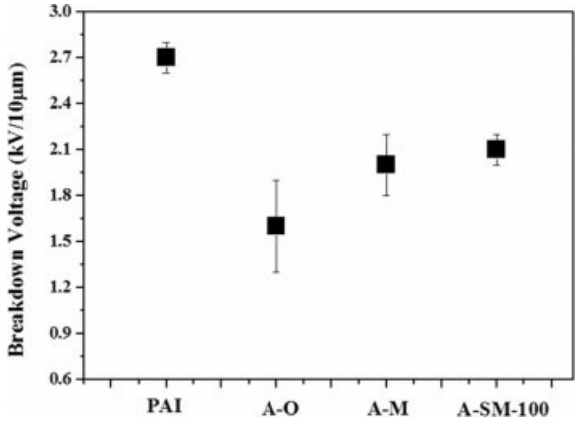


**Fig.7.** Breakdown strength of surface-modified α-$Al_2O_3$/PAI coating films.

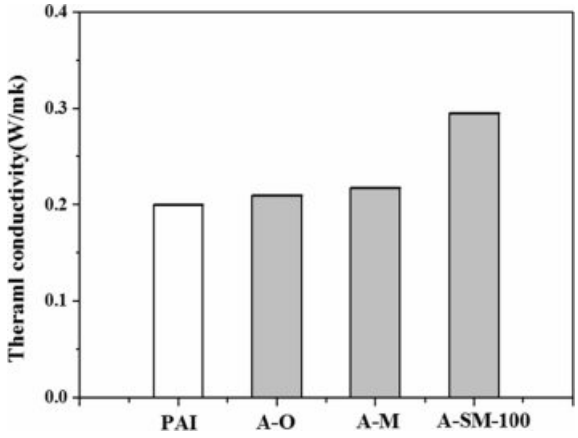


**Fig. 8.** Thermal conductivity of α-$Al_2O_3$/PAI hybrid composites.

The strength of $Al_2O_3$/PAI hybrid coating film was analyzed by breakdown voltage measurement in Fig. 7. For PAI alone, a breakdown voltage of approximately

2.7 kV was measured, while PAI coating film with A-O, A-M, and A-SM-100, which were used as nanofiller and the concentration was fixed at 20 wt%, showed breakdown voltages of 1.6, 2, and 2.1 kV, respectively. PAI coating film with A-O showed the rapid decrease of breakdown voltage because hydrophilic OH groups on the surface of α-$Al_2O_3$ particles caused the distance between the particles to decrease, which reduced the stability because of the formation of some aggregated particles within PAI. However, the insulation properties were enhanced despite the A-M particles having a greater increase in OH groups compared to the A-O particles. Because the nitric acid, which was used as an additive during the milling process, was adsorbed on the particle surface to add the repulsive force between some particles within the PAI resin. The film with A-SM-100 showed high insulation properties that were more enhanced compared to those of the A-O and A-M samples showing values that were similar to PAI resin alone because of the decrease in OH groups on the particle surface according to surface modifications.

Thermal conductivity of $Al_2O_3$/PAI hybrid coating films was measured and shown in Fig. 8. For PAI alone, the thermal conductivity was 0.20 W/mK, while those of A-O, A-M, and A-SM-100 samples were 0.21, 0.22, and 0.30 W/mK, respectively. The A-O sample interfered with heat flow because of some aggregated particles within PAI, while dispersibility in the A-M sample improved because of milling, as shown in Fig. 2. However, since there were no substances that could form direct bonds with PAI, no changes in thermal conductivity were found. On the other hand, the A-SM-100 sample showed enhanced heat flow between α-$Al_2O_3$ particles and PAI according to surface modifications, resulting in an increase in thermal conductivity of approximately 50% compared to PAI alone. It is believed that this is the result of the π-π interaction between PAI and the aromatic ring, which is the functional group of N-APTMS, contributing to adhesion properties with PAI.

## Conclusions

In order to enhance the thermal properties of PAI resin, α-$Al_2O_3$ with excellent thermal conductivity and insulation properties was used to produce alumina composite materials. The surface of α-$Al_2O_3$ nanoparticles were modified by the silane coupling agent with different content. Prior to surface modification, a milling process was performed to prepare a dispersed nano sol, which was subjected to surface modification according to the added amount of N-APTMS, a silane coupling agent. The properties of surface-modified $Al_2O_3$ nanoparticles were analyzed via TGA, wettability analysis, and PSA, which showed that the properties were in the order of A-SM-100 > A-SM-50 > A-SM-200. For identifying the amount adsorbed on the particle surface, the surface characteristics of the A-O, A-M, and A-SM samples were examined by comparing the surface hydroxyl groups through acid-base titration. The A-M sample showed a roughly 2.5-fold increase in surface hydroxyl groups due to size decrease. When the surface was modified with N-APTMS, the number of sites on the surface decreased in all cases. Moreover, compared to the A-O sample, the A-SM-100 sample had its sites covered completely by the surface hydroxyl groups, whereas the A-SM-200 sample showed a large increase in the number of sites. It was due to the silane content creating a difference in the speed of direct reaction with the $Al_2O_3$ particle surface and altering the amount being adsorbed on the particle surface, thereby controlling the dispersibility. The breakdown voltage and thermal conductivity of hybrid composite film increased in the order of A-SM-100 > A-M > A-O. The PAI composite film with A-SM-100, which represented surface treatment with an appropriate amount of silane coupling agent, showed the highest the enhancement of thermal and insulation properties due to the remarkable dispersibility of filler within PAI matrix.

## Acknowledgments

The authors gratefully acknowledge support for this study from the Energy Technology Development Project (20131020000130), Development of Electrical Insulation Nanohybrid Materials for Motor (Rectangular) Coil.

## References

1. A.C. Balazs, T. Emrick, and T.P. Russell, Science 314 (2006) 1107-1110.
2. M. Naffakh, A.M. Diez-Pascual, and M.A. Gomez-Fatou, J. Mater. Chem. 21 (2011) 7425-7433.
3. P.M. Ajayan, L.S. Schadler, and P.V. Braun, in "Nanocomposite science and technology" (John Wiley & Sons, 2006) p. 155.
4. W.R. Caseri, Mater. Sci. Tech. 22 (2006) 807-817.
5. K.I. Winey, and R.A. Vaia, MRS bull. 32 (2007) 314-322.
6. J. Jiang, G. Oberdorster, and P. Biswas, J. Nanopart. Res. 11 (2009) 77-89.
7. H. Zou, S. Wu, and J. Shen, Chem. Rev. 108 (2008) 3893-3957.
8. K.K. Nanda, A. Maisels, F.E. Kruis, H. Fissan, and S. Stappert, Phys. Rev. lett. 91 (2003) 106102.
9. W. Peukert, H.C. Schwarzer, and F. Stenger, Chem. Eng. Process. 44 (2005) 245-252.
10. S. Kango, S. Kalia, A. Celli, J. Njuguna, Y. Habibi, and R. Kumar, Prog. Polym. Sci. 38 (2013) 1232-1261.
11. L. Fang, C. Wu, R. Qian, L. Xie, K. Yang, and P. Jiang, RSC Adv. 4 (2014) 21010-21017.
12. M.G. Park, H. Kim, H.M. Lim, J.S. Choi, and D.S. Kim, Korean J. Mater. Res. 26 (2016) 136-142.
13. H.Y. Jo, D.S. Jung, S.H. Lee, D.S. Kim, Y.K. Lee, and H.M. Lim, Nanosci. Nanotechnol. Lett. 8 (2016) 21-26.
14. H.D. Lee, J.M. Kim, D.H. Son, S.H. Lee, and S.S. Park, Appl. Chem. Eng. 24 (2013) 391-395.

15. G.S. Cho, D.H. Lee, H.M. Lim, S.H. Lee, C.Y. Kim, and D.S. Kim, Korean J. Chem. Eng. 31 (2014) 2088-2093.
16. Y. Shinozaki, M. Tokieda, and K. Kawahara, U.S Patent Application No. 815369 (2006).
17. J.W. Ntalikwa, Bull. Chem. Soc. Ethiop. 21 (2007) 117-128.
18. Y. Wang, B. Du, X. Dou, J. Liu, B. Shi, D. Wang, and H. Tang, Colloids Surf. A: Physicochem. Eng. Aspects 307 (2007) 16-27.